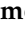





Article

Experimental Characterization of Hydrocarbons and Nitrogen Oxides Production in a Heavy-Duty Diesel–Natural Gas Reactivity-Controlled Compression Ignition Engine

Giacomo Silvagni ¹, Abhinandhan Narayanan ², Vittorio Ravaglioli ^{1,*}, Kalyan Kumar Srinivasan ², Sundar Rajan Krishnan ², Nik Collins ², Paulius Puzinauskas ² and Fabrizio Ponti ¹

¹ Department of Industrial Engineering—DIN, University of Bologna, 40126 Bologna, Italy; giacomo.silvagni2@unibo.it (G.S.); fabrizio.ponti@unibo.it (F.P.)

² Department of Mechanical Engineering, The University of Alabama, Tuscaloosa, AL 35487, USA; anarayanan2@crimson.ua.edu (A.N.); ksrinivasan@eng.ua.edu (K.K.S.); skrishnan@eng.ua.edu (S.R.K.); nscollins@crimson.ua.edu (N.C.); ppuzinauskas@eng.ua.edu (P.P.)

* Correspondence: vittorio.ravaglioli2@unibo.it

Abstract: Reactivity-Controlled Compression Ignition (RCCI) combustion is considered one of the most promising Low-Temperature Combustion (LTC) concepts aimed at reducing greenhouse gases for the transportation and power generation sectors. Due to the spontaneous combustion of a lean, nearly homogeneous mixture of air and low-reactivity fuel (LRF), ignited through the direct injection of a small quantity of high-reactivity fuel (HRF), RCCI (dual-fuel) shows higher efficiency and lower pollutants compared to conventional diesel combustion (CDC) if run at very advanced injection timing. Even though a HRF is used, the use of advanced injection timing leads to high ignition delays, compared to CDC, and generates high cycle-to-cycle variability, limited operating range, and high pressure rise rates at high loads. This work presents an experimental analysis performed on a heavy-duty single-cylinder compression ignited engine in dual-fuel diesel–natural gas mode. The objective of the present work is to investigate and highlight the correlations between combustion behavior and pollutant emissions, especially unburned hydrocarbons (HC) and oxides of nitrogen (NO_x). Based on the analysis of crank-resolved pollutants measurements performed through fast FID and fast NO_x systems under different engine operating conditions, two correlations were found demonstrating a good accordance between pollutant production and combustion behavior: Net Cyclic Hydrocarbon emission—cyclic IMEP variations ($R^2 = 0.86$), and Cyclic NO_x—maximum value of the Rate of Heat Released ($R^2 = 0.82$).

Keywords: LTC; RCCI; CO₂ reduction; dual fuel; fast FID; fast NO_x



Citation: Silvagni, G.; Narayanan, A.; Ravaglioli, V.; Srinivasan, K.K.; Krishnan, S.R.; Collins, N.; Puzinauskas, P.; Ponti, F. Experimental Characterization of Hydrocarbons and Nitrogen Oxides Production in a Heavy-Duty Diesel–Natural Gas Reactivity-Controlled Compression Ignition Engine. *Energies* **2023**, *16*, 5164. <https://doi.org/10.3390/en16135164>

Academic Editors: Tomasz Czakiert and Monika Kosowska-Golachowska

Received: 30 May 2023

Revised: 20 June 2023

Accepted: 3 July 2023

Published: 4 July 2023



Copyright: © 2023 by the authors. Licensee MDPI, Basel, Switzerland. This article is an open access article distributed under the terms and conditions of the Creative Commons Attribution (CC BY) license (<https://creativecommons.org/licenses/by/4.0/>).

1. Introduction

Over the recent years, thanks to a vast improvement in fast sensor and actuator technology and a profound understanding of the phenomena that affect the combustion process in IC engines, the feasibility of implementing cycle-by-cycle-based control to attain optimum engine performance and emissions is growing. With the push towards global decarbonization growing stronger, a combination of advanced combustion strategies and effective next-cycle control could be a pivotal pathway towards meeting the stringent emissions regulations for IC engines. Researchers have demonstrated the abilities of technologies like Homogeneous Charge Compression Ignition (HCCI) [1,2], Premixed Mixture Ignition in the End-gas Region (PREMIER) [3,4], pre-chamber combustion systems [5,6] and Reactivity-Controlled Compression Ignition (RCCI) [7,8] to produce high fuel conversion efficiencies while maintaining low engine-out emissions. Of these, the RCCI/dual-fuel Low-Temperature Combustion (LTC) strategy has proven to be a viable pathway to achieve ultra-low NO_x emissions and good fuel conversion efficiencies (FCE) at both high and low

load operations [9–16]. Hariharan et al. [17] experimentally studied the effect of various engine operating parameters like injection timing, intake pressure and injection pressure on emissions and performance of dual-fuel combustion with diesel–natural gas (NG) and polyoxymethylene di-methyl ether (POMDME)–NG as fuel combinations. At low loads (~5 bar IMEP), the authors were able to achieve indicated FCEs of >40% and indicated specific NO_x values of ~0.1 g/kWh at injection timings ranging from 40–60 deg bTDC. However, these single-injection operating points were found to have high cyclic variations and high HC emissions. The authors were able to mitigate the negative impact of cyclic variations by adding a second injection closer to TDC and by operating at lower intake pressures. Cyclic variations, which arise due to fluctuations in local air fuel ratios and in-cylinder thermodynamics, have a profound negative impact on HC emissions and engine performance. Methods to quantify cyclic variations and to identify its cause have been extensively documented in the literature [18–23]. For example, Jha et al. [24] experimentally examined the effect of methane energy fraction at low loads in diesel–methane dual fuel combustion at early injection timings. They observed that increasing the energy fraction of methane from 50% to 90% at –50 deg aTDC start of injection decreased NO_x emissions by a factor of 43; increased HC emissions by a factor of 9 and increased cyclic variations. The authors attributed the increase in cyclic variations to the decrease in reactivity of the mixture as methane energy fraction increases. Various diagnostics methods have been investigated to examine cyclic variations in dual fuel combustion. Cheng et al. [25] examined cyclic variations in diesel–methane dual fuel combustion using optical methods and used a proper orthogonal decomposition method to analyze and quantify cyclic variations. The increased fluctuations in the luminosity field were considered to be a marker for increased cyclic variations. They observed delayed onset of cyclic variations as the methane fraction increased at an injection timing of 15 deg bTDC.

The objective of the present work is to correlate the cause of high HC and NO_x emissions to the combustion behavior in diesel–NG dual fuel combustion using cyclic emissions data obtained from fast pollutant measurement systems in combination with combustion data.

2. Experimental Setup

Experimental studies were performed on a single cylinder version of a heavy-duty PACCAR MX11 engine setup at the University of Alabama (UA). The engine specifications are provided in Table 1. The Single-Cylinder Research Engine (SCRE) was coupled to a 393 HP AC dynamometer and a Dyne Systems IL5 controller was used to control the engine speed, while engine load (as determined by the Indicated Mean Effective Pressure (IMEP)) was set by controlling fueling rates.

Table 1. Engine technical characteristics.

Engine Parameter	Values
Engine type	Single cylinder, four-stroke
Displaced volume	1.806 m ³
Maximum Torque	350 Nm @ 1000 rpm
Maximum Power	53 kW @ 1750 rpm
Injection System	Common Rail Injection system
Bore	123 mm
Stroke	152 mm
Compression ratio	18.5:1
Intake Valve	IVO: 350 deg aTDC, IVC: –150 deg aTDC
Exhaust Valve	EVO: 130 deg aTDC, EVC: –355 deg aTDC
Maximum Speed	2200 rpm
Maximum Pressure	245 bar

A common rail direct injection system was used to inject the High-Reactivity Fuel (HRF) and the rail pressure was controlled using a solenoid actuated inlet metering valve

and rail pressure control valve. A National Instruments Direct-injector Control and Measurement device (DCM) interfaced with the Calibration Viewer software from Viatech and was used to control injection timing and injection duration. The Low-Reactivity Fuel (LRF) was fumigated along with the intake air and the LRF flowrate was controlled using a Swagelok KLF series pressure regulator. The fuel flowrates were measured using Emerson Micromotion Coriolis flowmeters.

The intake air system uses an external air compressor which also conditions the high-pressure air (up to 5 bar) using a heatless desiccant dryer. The intake air mass flowrate was measured using a sonic nozzle, for which the pressure and temperature upstream of the nozzle were also measured to compute the air mass flowrate. The upstream pressure was measured using a Setra 206S pressure transducer and the temperature was measured using an Omega K-type thermocouple. A Kistler piezoelectric pressure transducer (6124A) coupled with a charge amplifier (5018) was used to measure the in-cylinder pressure, and the dynamic pressures of both the intake and exhaust were measured using Kistler piezoresistive pressure transducers. The in-cylinder pressure profile was phased using a BEI shaft encoder with 0.1 CAD resolution.

Cycle-resolved HC and NO_x were obtained by installing CMBUSTION HFR400 FID (Fast FID) and CMBUSTION CLD500 (Fast NO_x) measurement systems in the exhaust manifold, respectively (as close as possible to the exhaust port). By using the Fast FID and Fast NO_x systems, which can sample the pollutants at 500 Hz, it was possible to obtain the “instantaneous” emissions for each engine cycle. As a result, since the output of such measurement systems were phased with the data acquisition system, it was possible to link the cylinder pressure trace during the combustion process and the respective pollutant production in a given cycle.

Moreover, to compare the present data with the literature, slow-speed (1 Hz) pollutant measurements were also performed by using a NOVA 5466 AK gas analyzer (present in a standard Richmond five-gas emission bench) and a CONTINENTAL UniNO_x SNS14 sensor (100 Hz) mounted close to the Fast NO_x probe. Figure 1 shows the UA SCRE test cell layout used for the present experimental efforts.

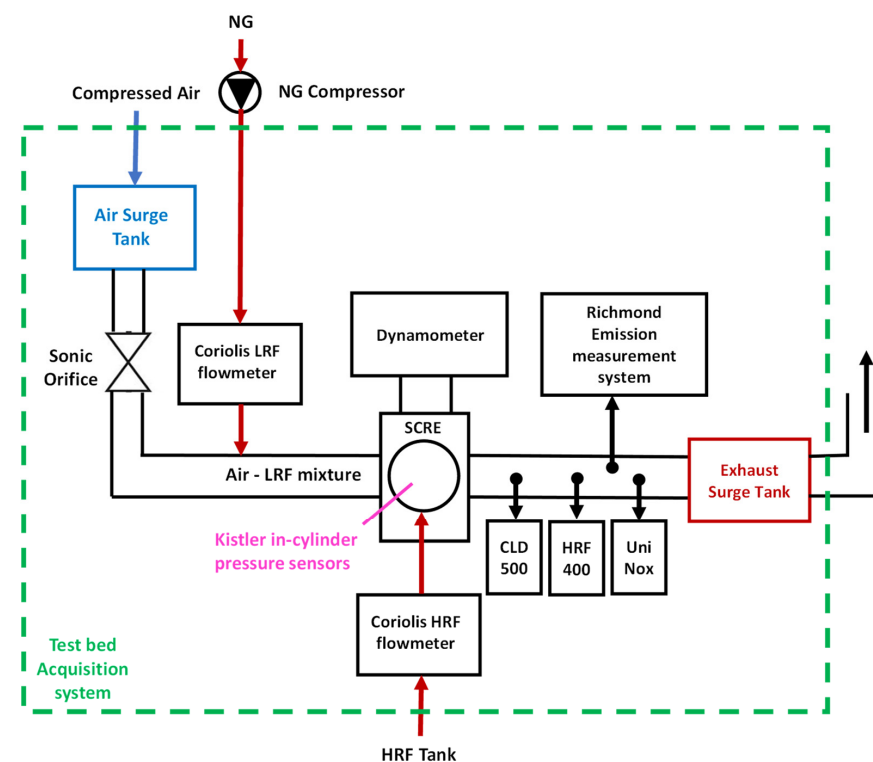


Figure 1. A schematic representation of the UA single-cylinder research engine setup used for the present experiments.

3. Experimental Methodology

As widely reported in the literature [26,27] and explained later in this paper, to achieve high combustion efficiencies with dual-fuel combustion, an early Start of Injection (SOI) is needed. With early SOIs, the shape of the apparent rate of heat release (RoHR) curve is “Gaussian” and it generates very low pollutants, especially NO_x, and high indicated efficiency. However, dual-fuel combustion at very advanced SOIs leads to the ignition process (dictated by the HRF injection) becoming driven more by in-cylinder chemical reactions that are especially driven by the local air–fuel ratio [28–30]. By using advanced SOIs, the HRF ignition delay increases due to the local air–fuel ratio “over leaning”, and it generates engine instability as evident from high values of the coefficient of variation (COV) of indicated mean effective pressure (IMEP).

To better highlight differences in combustion RoHR shapes, efficiency, and pollutant emissions in dual-fuel combustion, two SOI sweeps were performed, operating the SCRE at low loads, where HC emissions are exacerbated. To highlight the link between cyclic HC emissions and combustion instability, highly unstable engine operating conditions were specifically studied. Moreover, to better understand the reason behind the NO_x production with dual-fuel combustion, different boost pressures and percent energy substitution (PES) of natural gas were considered. The engine operating conditions presented in this paper are summarized in Tables 2 and 3. The experimental studies were performed at a speed of 1339 RPM, which was identified as the “B-speed” of the original PACCAR MX-11 engine and 1000 cycles of data were collected for each operating point. For the analyzed SOI sweeps, the injection pressure was kept at 500 bar, and the PES was maintained at 80% and 75%, respectively. The PES was computed using Equation (1).

$$\text{PES} = \frac{\dot{m}_{\text{LRF}} \text{LHV}_{\text{LRF}}}{\dot{m}_{\text{HRF}} \text{LHV}_{\text{HRF}} + \dot{m}_{\text{LRF}} \text{LHV}_{\text{LRF}}} \quad (1)$$

Table 2. Engine operating conditions that were chosen to study the impact of cyclic variations on HC emissions at Intake Pressure 1.5 bar, Intake Temperature 20 °C, IMEP 5 bar and PES 80%.

SOI [deg aTDC]	Intake Pressure [bar]	Intake Temperature [°C]	PES [%]	COV IMEP _g [%]
−10	1.5	20	80	6
−20	1.5	20	80	5.7
−30	1.5	20	80	3.8
−40	1.5	20	80	6.3
−50	1.5	20	80	17.1
−60	1.5	20	80	22

Table 3. Engine operating conditions that were chosen to study the impact of cyclic variations on NO_x emissions at Intake Pressure 1.48 bar, Intake Temperature 20 °C, IMEP 5 bar and PES 75%.

SOI [deg aTDC]	Intake Pressure [bar]	Intake Temperature [°C]	PES [%]	COV IMEP _g [%]
−10	1.48	20	75	7.4
−15	1.48	20	75	8.2
−20	1.48	20	75	6.3
−25	1.48	20	75	4.8
−30	1.48	20	75	3.6
−35	1.48	20	75	4.7
−40	1.48	20	75	5.9
−45	1.48	20	75	7.6
−50	1.48	20	75	11

To study in depth the combustion process at different engine conditions, the RoHR, the cumulative heat release, and the main combustion indexes, such as IMEP, location (CAD) of 50% heat release (CA50), Peak Pressure Rise Rate (PPRR), were calculated starting from Equation (2) (γ represents the specific heat ratio, V and p are the combustion chamber volume and pressure, respectively, and dV and dp are their derivatives) [31] for each engine cycle:

$$ROHR = \frac{1}{\gamma - 1} \cdot V \cdot \frac{dp}{d\theta} + \frac{\gamma}{\gamma - 1} \cdot p \cdot \frac{dV}{d\theta} \quad (2)$$

The Start of Injection (SOI) was swept from a retarded injection timing of -10 deg aTDC to an advanced injection timing of -50 deg aTDC at constant intake and rail pressures.

Figure 2 shows the impact of the SOI on the average CA50 at a constant IMEP of approximately 5 bar running the sweep described in Table 3. The trend reported in Figure 2 clearly shows the typical behavior during the transition between a typical two-stage profile to a Gaussian profile for dual-fuel combustion in terms of the “switchback” of CA50 direction with respect to the SOI [26,32]. The reason of the SOI-CA50 trend shown in Figure 2 is related to the fact that advancing the angular position of the diesel injection within the cycle increases the ignition delay because of different charge thermodynamic conditions [28,30].

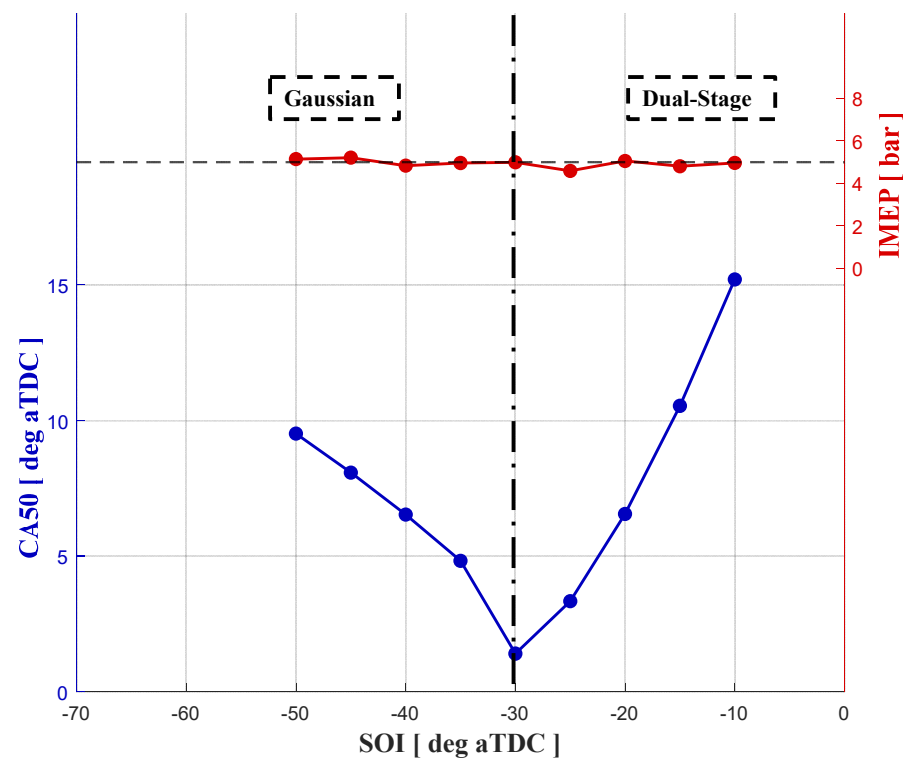


Figure 2. Average CA50 and IMEP measured during the SOI sweep at a constant IMEP of 5 bar.

To better explain the SOI-CA50 trend, the difference in combustion RoHR shapes during the SOI sweeps at the same load (5 bar IMEP) are shown in Figure 3. As evident from this figure, starting from SOI -10 to SOI -30 deg aTDC the combustion shows the typical dual-stage RoHR shape: a first peak in RoHR generated by the combustion of a relatively non-homogeneous air–fuel mixture related to the HRF injection then followed by combustion in the more homogeneous natural gas–air mixture. As has been widely documented in the literature [3], such behavior is generated by very short ignition delay of the HRF when injected close to TDC (the air–fuel mixture pressure, temperature, and the charge stratification are high). After the first combustion phase, the RoHR reported in Figure 3a shows the typical second RoHR stage is characterized by smoother and slower

energy release process, due to the combustion of the LRF–air mixture far from the stratified zone. Based on the previous explanation, running the engine with late SOIs, from -30 to -10 deg aTDC, CA50 and SOI follow the same movement direction because of the very short HRF ignition delay and favorable charge thermodynamic conditions (Figure 2, right side).

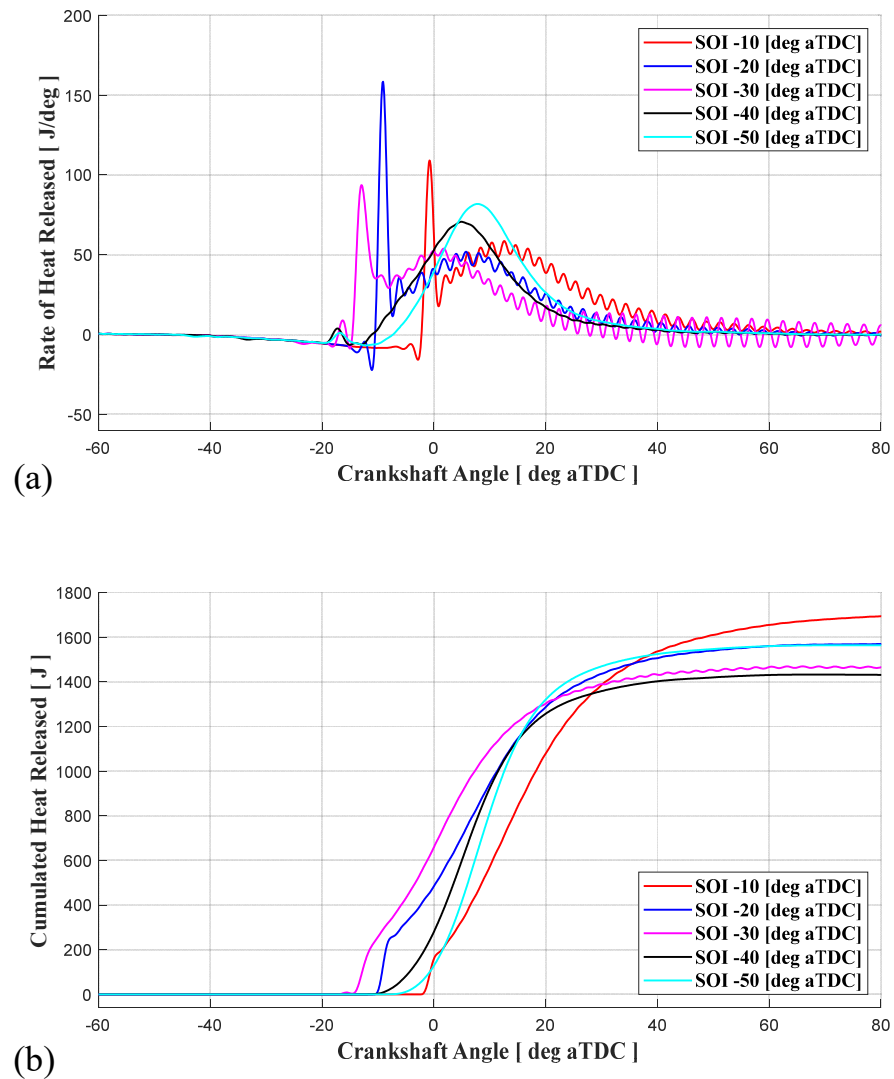


Figure 3. (a) Rate of Heat Release, and (b) Cumulate Heat Released curves testing different SOI at the same load (5 bar IMEP), PES (80%), and boost pressure 1.5 bar.

A further advance in SOI, from -30 to -50 deg aTDC, produces a completely different behavior, characterized by a smoother single-stage combustion RoHR that appears “Gaussian” in shape. On the contrary, running the engine with early SOIs, the CA50 retards when the SOI advances (Figure 2, left side). Due to the extremely unfavorable LRF–air mixture thermodynamic conditions when the HRF is injected at early SOIs, the HRF ignition delay increases, allowing for greater HRF mixing with the LRF–air mixture and avoiding the creation of stratified zones close to the injector tip. This enhanced mixing leads to a relatively slower and smoother combustion process characterized by the single-stage Gaussian RoHR curve. It is important to highlight the presence of the Low-Temperature Heat Release (LTHR), approximately at -16 deg aTDC, which represents a well-known phenomenon [33] often visible in single-stage dual-fuel combustion.

Moreover, from Figure 3a, it is important to observe the presence of remarkable RoHR oscillations during the expansion stroke when the engine was run at a retarded SOI, from -10 to -30 deg aTDC. Such a phenomenon is typically triggered by the pressure waves

generated by an impulsive combustion process, such as the first stage combustion in Figure 3a [34]. Such a very short and intense energy release increases the amplitude of the resonance frequencies related to the vibrational mode of the combustion chamber. To better analyze this aspect, further analysis is currently being performed.

As has been well documented by the literature [35], the transition from two-stage to Gaussian single-stage combustion produces remarkable differences both in terms of pollutants and efficiency. Figure 3b, which shows the ensemble-average Cumulated Heat Released (CHR) at different SOIs, confirms that even if the CA50 has been varied, the load has been kept almost constant (maximum CHR close to 1500 J). Figure 4 shows the average Indicated Specific Fuel Consumption (ISFC) in terms of diesel-equivalent ISFC and the main pollutant emissions (total HC, CO and NOx) sampled by the Richmond gas analyzer during each test.

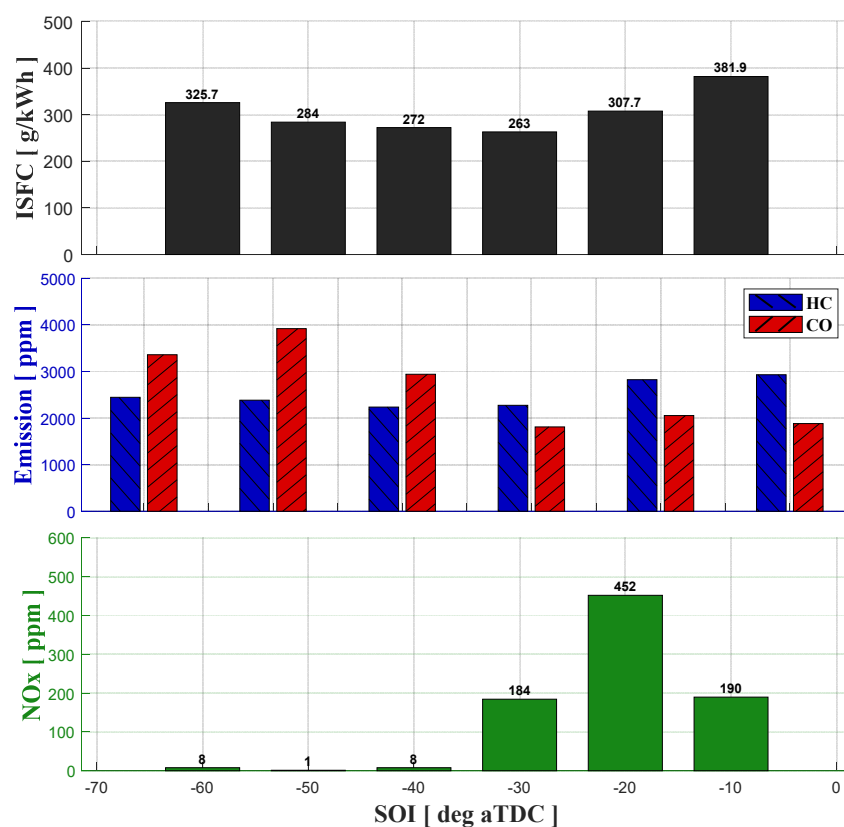


Figure 4. ISFC and pollutants (HC, CO and NOx) production during the SOI sweep running the SCRE engine in dual-fuel mode at low load (IMEP 5 bar), 75% PES, and boost pressure 1.48 bar. Note: For ease of comparison and because the nominal load was held constant at IMEP = 5 bar, steady-state emissions are presented in raw units (ppm) instead of the customary brake-specific units.

From Figure 4, typical ISFC and emissions trends are observed. The increase in NOx is linked to the more locally stratified combustion leading to higher local temperatures, while ISFC and HC reductions are linked to higher combustion efficiencies. It is important to highlight that even if the CA50 was around maximum brake torque (MBT) or maximum IFCE location for standard ICEs (i.e., 5–7 deg aTDC at SOI equal to -30 deg aTDC), the two-stage RoHR and the associated stratified combustion (from SOI -10 to -30 deg aTDC) are characterized by high NOx emissions. As a result, despite its benefit in combustion controllability through the injection position, the two-stage RoHR shows limitations in reaching both goals simultaneously.

Since the aim of dual-fuel combustion is to drop both emissions and fuel consumption as much as possible, further advance in SOI generates a Gaussian combustion and it shows the best tradeoff in pollutants and efficiency. The experimental evidence reported in Figure 4

is well-supported by data available in the dual-fuel literature [26,27]. A smooth combustion characterized by CA50 close to MBT produces very low NOx. A further increment in SOI generates a slight rise in ISFC and HC mainly because the CA50 occurs later as the piston is further down the expansion stroke. Furthermore, the CO generation increases mainly because the CA50 is retarded, the combustion duration increases with a direct impact in lowering the exhaust temperature. Figure 5 shows ISFC and pollutants emissions for engine operation at a slightly higher PES of 80% and boost pressure 1.48 bar. As expected, even at slightly higher PES, SOI variations exhibit similar trends.

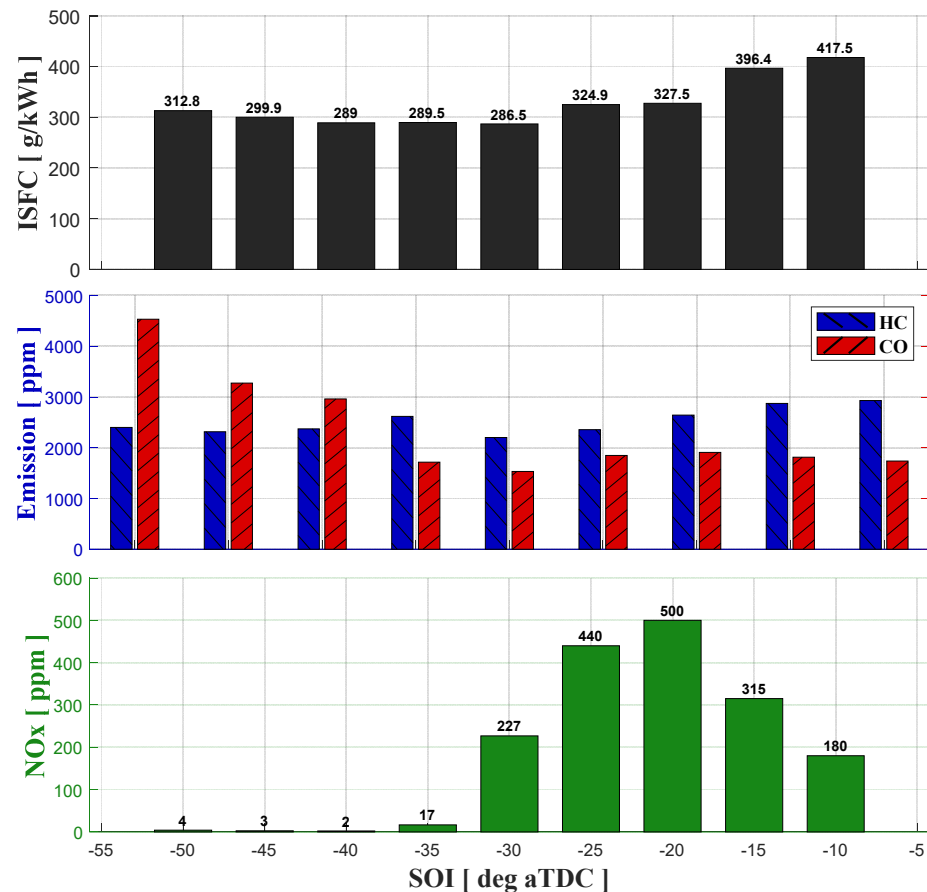


Figure 5. ISFC and pollutants (HC, CO and NOx) production during the SOI sweep running the SCRE engine in dual-fuel mode at low load (IMEP 5 bar), 80% PES, and boost pressure 1.5 bar.

Despite previous efforts in which the authors demonstrated significant reductions in fuel consumption and pollutants by performing a “calibration style” parametric study [17], this work is focused on demonstrating the links between high HC and NOx emissions and the combustion process. Therefore, the focus is specifically not on determining the “best operating point” with dual-fuel combustion.

The following section demonstrates the links between the combustion indices and the information obtained from the high frequency (cycle-resolved) pollutants measurements with low-load dual-fuel combustion.

4. Results and Discussion

To analyze the impact of the combustion characteristics on cycle-resolved pollutants production, attention was focused on those operating conditions that led to high cycle-to-cycle variability (and associated high HC emissions) and to high NOx emissions.

4.1. Cyclic HC—IMEP Correlation

As described in the Introduction, one of the aims of this work is to demonstrate the correlation between the cyclic HC production and IMEP (gross) by using a crank-resolved measurement system operating the heavy-duty SCRE in dual-fuel mode.

Our previous efforts [17] demonstrated that despite remarkable improvements in pollutant emissions and fuel consumption reduction possible with dual-fuel combustion at very advanced SOI, the combustion stability is strongly influenced by the PES and the thermodynamic conditions of the air–fuel mixture. As a result, through the analysis of the experimental data acquired during the performed SOI sweeps, to find out the HC–IMEP correlation it was decided to focus the attention on the 80% PES tests described in Figure 4.

The two engine operating points identified to highlight this correlation are characterized by approximately the same IMEP and CA50 but very different COV of IMEP (we discuss this aspect later in the paper). As reported in Figure 6, the spread of the cyclic IMEP and CA50 are seen by analyzing a subsystem of 300 consecutive cycles (same considerations can be extended to the entire dataset) in the two identified engine conditions at low load: “Advanced SOI” (SOI -60 deg aTDC) and “Retarded SOI” (-10 deg aTDC).

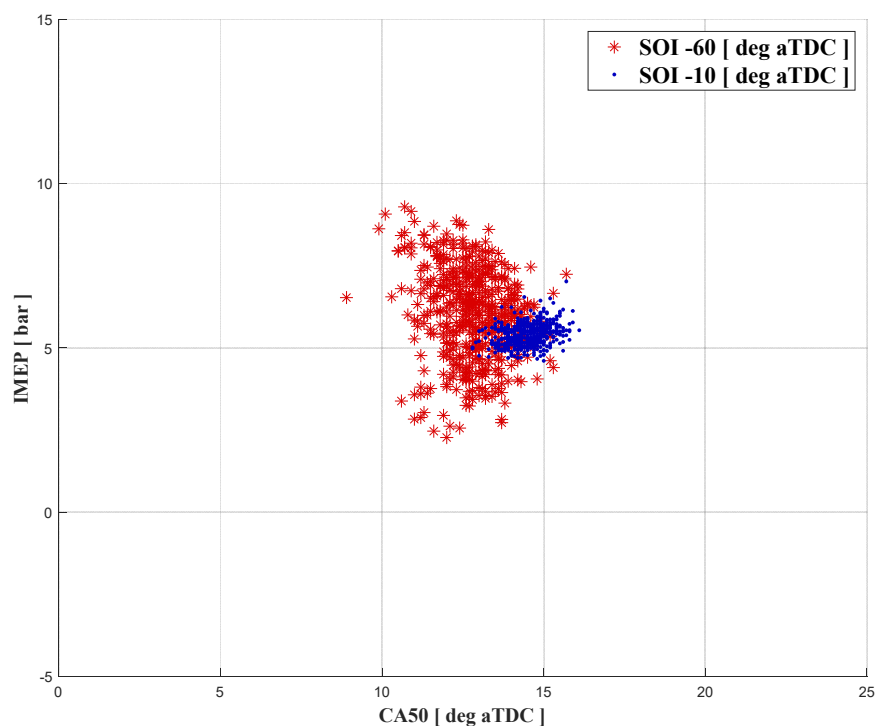


Figure 6. Comparison between measured cyclic CA50–IMEP gross (300 engine cycles) related to two different engine conditions: SOI -60 deg aTDC called “Advanced SOI”, and SOI -10 deg aTDC called “Retarded SOI”.

For dual-fuel combustion at very advanced SOI, the ignition process (as discussed previously) is driven more by in-cylinder chemistry, which in turn, is affected by the local air–fuel ratio [26–30,36]. To better clarify this aspect, the cyclic IMEP of two groups of 300 consecutive cycles with different SOIs (“Retarded SOI” and “Advanced SOI”) are shown in Figure 7. By using advanced SOI, the HRF ignition delay increases due to the “over leaning” of local air–fuel ratios, and this leads to high COV. The spread of CA50 instead is related to the presence of recovery cycles after “near-misfire” engine cycles. After a very low-efficiency combustion, the residuals are mostly composed by unburned air–fuel mixture (fully premixed, after the entire exhaust and the intake stroke). Such extra chemical power given by the residuals increases the engine load anticipating the CA50 of the following cycle (“recovery cycles”) consequently. Such behavior is summarized

in Figure 8, where the two random groups of engine cycles (the group are highlighted through the yellow box) highlighted in Figure 7 are reported. As explained in the previous section of the paper, due to the different thermodynamic conditions when the HRF is injected, the two extreme SOIs are characterized by extremely different cyclic variations and combustion shape. It is important to mention that, using the AC dynamometer with its associated speed controller (Figure 1), it was possible to investigate extremely unstable engine conditions while keeping the engine speed at a constant value (engine speed fluctuations were mitigated by the dynamometer speed controller).

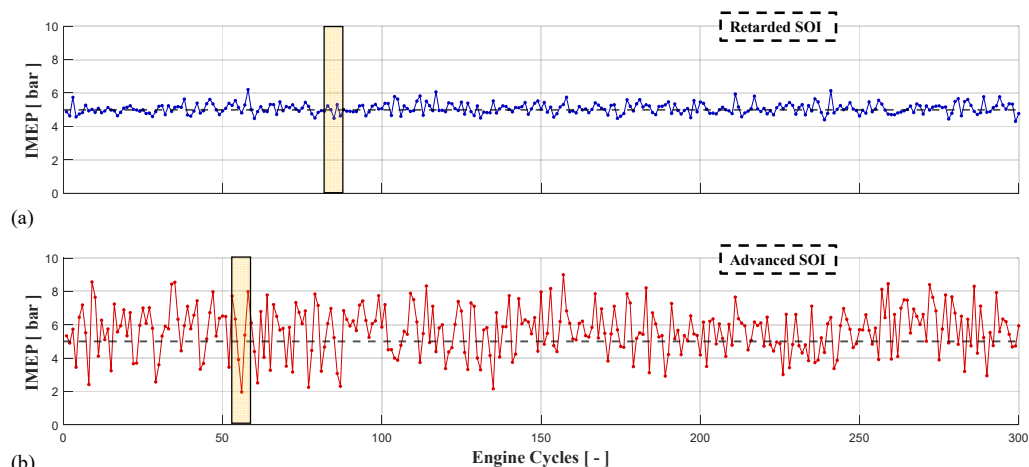


Figure 7. Measured IMEP for 300 consecutive engine cycles: (a) “Retarded SOI” condition, (b) “Advanced SOI” condition.

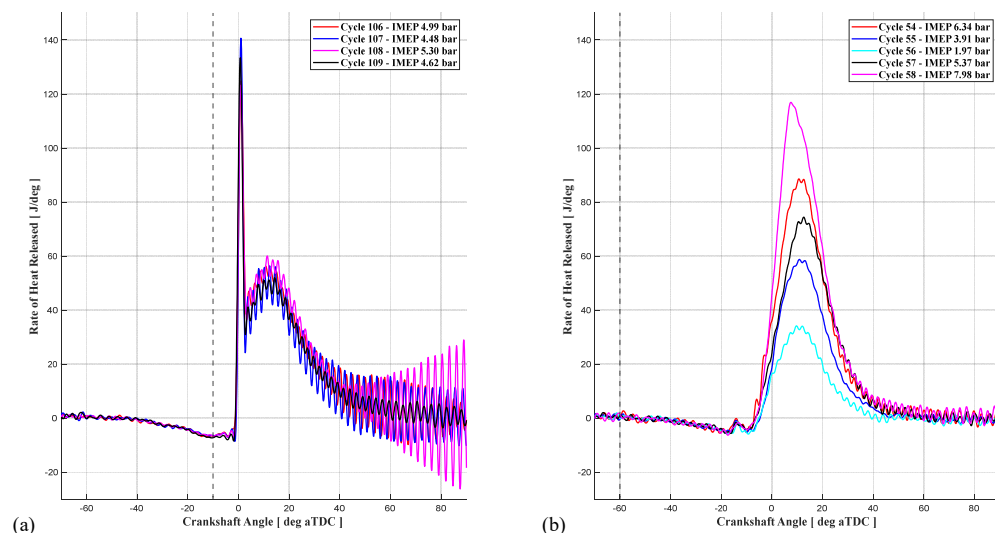


Figure 8. Measured Rate of Heat Released (RoHR) for consecutive cycles in the two different analyzed engine conditions: (a) “Retarded SOI”, dual-stage combustion, (b) “Advanced SOI”, “Gaussian” combustion.

As is evident from Figures 7 and 8, due to the different ignition dynamics and consequently combustion RoHR shape and duration, the two analyzed conditions clearly differ in terms of cyclic IMEP behavior: the “Retarded SOI” condition is characterized by very low COV (Figures 7a and 8a) whereas significant IMEP variations are observed for the “Advanced SOI” condition (Figures 7b and 8b).

To demonstrate the impact of the cyclic variations on HC production, cycle-resolved HC emissions were measured using a CAMBUSTION HFR400 fast FID analyzer. By using the fast FID measurement system, which can sample the hydrocarbon emissions at 500 Hz, it was possible to obtain the cycle-resolved HC emissions for each engine cycle. By running

the engine at 1339 rpm, the 500 Hz measurement frequency of the fast FID system led to a crank angle resolution of 16 degrees for the cycle-resolved HC measurements. As a result, since the output of the fast FID measurement system was phased with the data acquisition system, it was possible to link the cylinder pressure trace during the combustion process and the respective cycle's HC emissions.

Figure 9 shows the in-cylinder pressure signal for a single engine cycle and the associated fast FID signal. To improve the quality of the fast HC and fast NO_x visualization and analysis, a Butterworth low-pass digital filter (300 Hz) has been applied to the FID output.

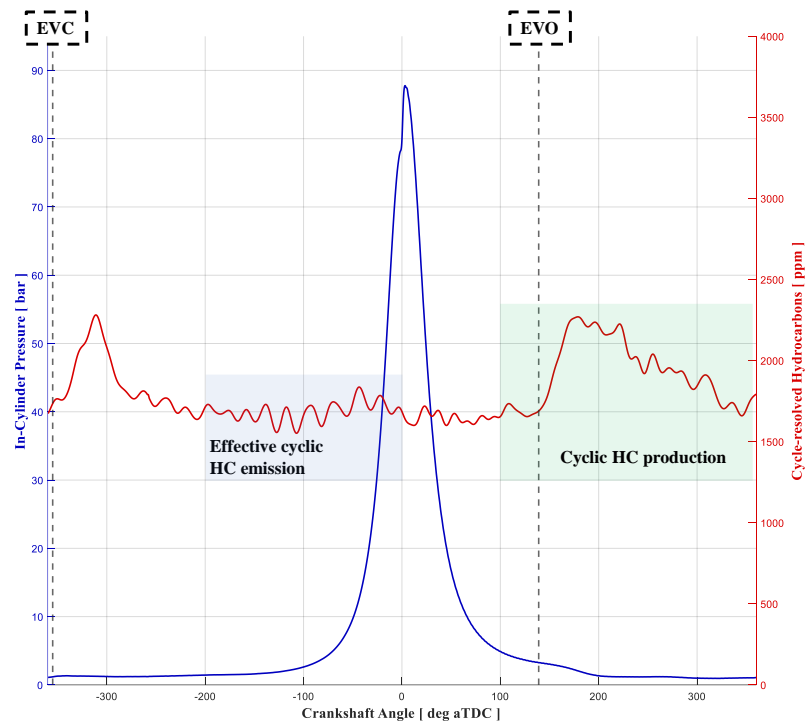


Figure 9. In-cylinder pressure signal and measured cycle-resolved HC emissions for dual-fuel operation at SOI -10 deg aTDC.

It is important to mention that due to the distance between the FID probe and the exhaust port, the fast FID signal is intrinsically characterized by a time-delay (approximately 0.0125 sec in the analyzed conditions) with respect to the exhaust valve opening. Since the analyzed engine operating conditions were run at a constant RPM and under the hypothesis that the exhaust gases pass through the exhaust manifold at the sound speed (i.e., under choked conditions) during the exhaust blowdown process, which can approximately be considered proportional to the square root of the exhaust gas temperature, the time-delay was compensated, and the fast FID signal was synchronized with the exhaust valve opening (EVO) for each cycle. As it can be seen in Figure 9, the instantaneous HC signal starts rising after EVO and, therefore, the information contained in the fast FID signal can be directly correlated with the analyzed cylinder pressure signal.

By the analysis of the instantaneous HC signal (Figure 9), three regions are noticeable, which provide different information about the HC emissions arising from the engine cycle. The first HC peak, located between -360 and -260 deg aTDC, is related to short-circuiting of natural gas from the intake directly to the exhaust. Despite the overlap window of the engine being very small (15 deg), because of the pressure difference between intake and exhaust, a small quantity of LRF-air mixture flows in the cylinder directly to the exhaust, causing the reported peak. The second region can be considered representative of the actual cyclic HC production (green area highlighted in Figure 9) during the combustion process. This area is characterized by the maximum value of instantaneous HC, which is directly related to the HC production during and after the combustion, and a clear

descending trend. Such a trend can be reasonably explained through the exhaust gases mixing process in the exhaust manifold during the expansion (the HC concentration lowers progressively). As a result, the cyclic HC production can be evaluated as the average of the fast FID signal during the exhaust stroke (green area in Figure 9). This value represents the “effective cyclic HC emissions” for the following engine cycle. Since the aim of this work is to correlate the IMEP cyclic variations with the HC emissions, the effective cyclic HC emissions was evaluated by averaging the FID signal (blue area highlighted in Figure 9) during the compression stroke, when both intake and exhaust valves are closed. Then, the Net Cyclic HC emission (NCHC), defined by Equation (3), was evaluated as the difference between the cyclic HC production (average of the green area in Figure 9) and the effective cyclic emissions for each engine cycle (average of the blue area in Figure 9).

$$\text{Net Cyclic HC emission [ppm]} = HC_{\text{cyclic production}} - HC_{\text{effective cyclic emission}} \quad (3)$$

The *NCHC* represents the net *HC* production (if positive), or the net *HC* reduction (if negative), for the analyzed engine cycle compared to the previous one. As a result, through the *NCHC* evaluation it is possible to obtain an index that can be easily correlated with the cyclic *IMEP* variation. To evaluate the cyclic *IMEP* variations, the ΔIMEP , defined in Equation (4), was calculated as the difference between the *IMEP* of two consecutive engine cycles.

$$\Delta\text{IMEP [bar]} = \text{IMEP}_{n_{th,cycle}} - \text{IMEP}_{(n-1)_{th,cycle}} \quad (4)$$

Once *NCHC* and ΔIMEP were defined, the cyclic *HC*– ΔIMEP correlation was obtained by the comparison between the two engine operating conditions considered in this work: “Retarded SOI” and “Advanced SOI”. Figure 10 clearly shows that a net *HC* reduction is related to a more efficient combustion process (positive ΔIMEP). On the other hand, if the combustion decreases in efficiency (negative ΔIMEP) the *NCHC* increases. It is interesting to notice that even if the spread of the *IMEP* is extremely different (because of differences in the nature of combustion at the two SOIs as evident from the different RoHR shapes), the correlation between the *NCHC* and the ΔIMEP is still valid for both analyzed engine conditions. Therefore, it appears that the obtained linear correlation ($R^2 = 0.86$) gives a reasonable indication about one the main source of *HC* production in RCCI engines and the relation between the cyclic variability and *HC* emissions in diesel–NG dual-fuel combustion.

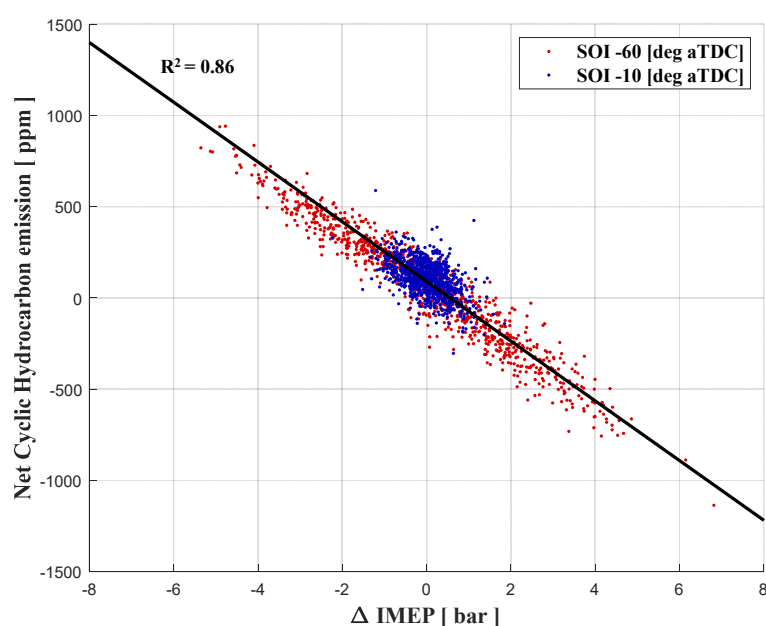


Figure 10. Cyclic HC–IMEP correlation for 300 consecutive cycles in the two different analyzed engine conditions: SOI –60 deg aTDC called “Advanced SOI” and SOI –10 deg aTDC called “Retarded SOI”.

4.2. Cyclic NO_x–RoHR_{max} Correlation

As has been widely reported in the literature [27,35], one of the main challenges with adapting dual-fuel combustion for the entire speed–load range production engines is related to the control of the combustion. Despite the fact that Gaussian RoHR shape at advanced SOIs is accompanied by very low NO_x and high efficiency, its high sensitivity to in-cylinder thermodynamic conditions and the SOI position significantly reduces the operating range of the engine. As a result, to increase the combustion controllability avoiding knock or misfire, previous efforts proposed retarded SOI operation for a certain number of engine cycles [17,26,35]. By using such SOI actuation, the engine can instantaneously recover from anomalous combustion events, preventing failures or damage to other components, such as the turbocharger, exhaust line, auxiliaries, etc.

Even though retarding the SOI can be considered an effective way to mitigate the well-known dual-fuel combustion, especially knock, moving from a single-stage Gaussian RoHR to a two-stage RoHR increases the NO_x emission. As reported in Figure 3a and confirmed by pollutants emissions shown in Figure 4, the two-stage combustion (SOI from -10 to -30 deg aTDC) is characterized by a very sharp first combustion stage and high NO_x production. As mentioned before, such behavior is generated by the very short ignition delay of the HRF when injected close to TDC (pressure, temperature and the stratification of the air–fuel mixture are high) which ignites the amount of charge in the stratified zone.

Since NO_x formation is driven by local temperatures potentially caused by the local air–fuel ratio stratification in dual-fuel combustion, RoHR calculated using a global combustion model is not directly referable to NO_x emissions. This is made even more difficult especially when the nature of combustion changes significantly (i.e., from two-stage to single-stage Gaussian RoHR).

However, because the NO_x production is promoted when a significant amount of energy is released in a short time, the link between the combustion behavior and the measured NO_x can be obtained by examining combustion indices related to knock. Typically, such information can be easily obtained by the analysis of the RoHR, and in particular its maximum value.

From Figure 3a, it is evident that for combustion characterized by two-stage RoHR (SOI from -10 to -30 deg aTDC), the maximum value of the RoHR (RoHR_{max}), typically occurring in the first stage, is significantly and consistently higher with respect to the more advanced SOIs (SOI from -40 to -50 deg aTDC). Figure 11 shows the steady-state (slow-speed) NO_x emissions measured with the Richmond bench and the RoHR_{max} (300 cycles) during the SOI sweep. It is evident that both NO_x and RoHR_{max} follow the same trend, demonstrating a potential link between the identified combustion parameter and NO_x production.

Focusing the attention on the SOI range characterized by two-stage combustion (SOI from -10 to -30 deg aTDC), because the first combustion stage progressively becomes more intense (Figure 2a), both NO_x and RoHR_{max} increase. The reported trend is generated by the decreasing HRF ignition delay, which promotes local air–fuel ratio stratification and higher local temperatures inside the combustion chamber. A further advancement in SOI (from -35 to -50 deg aTDC) modifies the RoHR shape, characterized by a smoother energy release (Gaussian profile). Such behavior is mainly related to the HRF ignition delay increment because of the unfavorable thermodynamic conditions in the combustion chamber when the HRF is injected [28,29]. The very low NO_x emissions shown by Figure 11 at advanced SOIs confirms a potential link between the combustion shape (i.e., the existence of a distinct first stage of RoHR) and NO_x emissions. It is important to highlight that the RoHR_{max} tends to increase when SOI is advanced because the center of combustion moves to MBT (Figure 2). A further confirmation of this trend can be found by the information shown in Figure 4, where ISFC and pollutants are reported.

Upon identification of the link between RoHR_{max} and NO_x emissions using the ensemble-averaged RoHR data and slow-speed NO_x measurements, cycle-to-cycle analysis was performed.

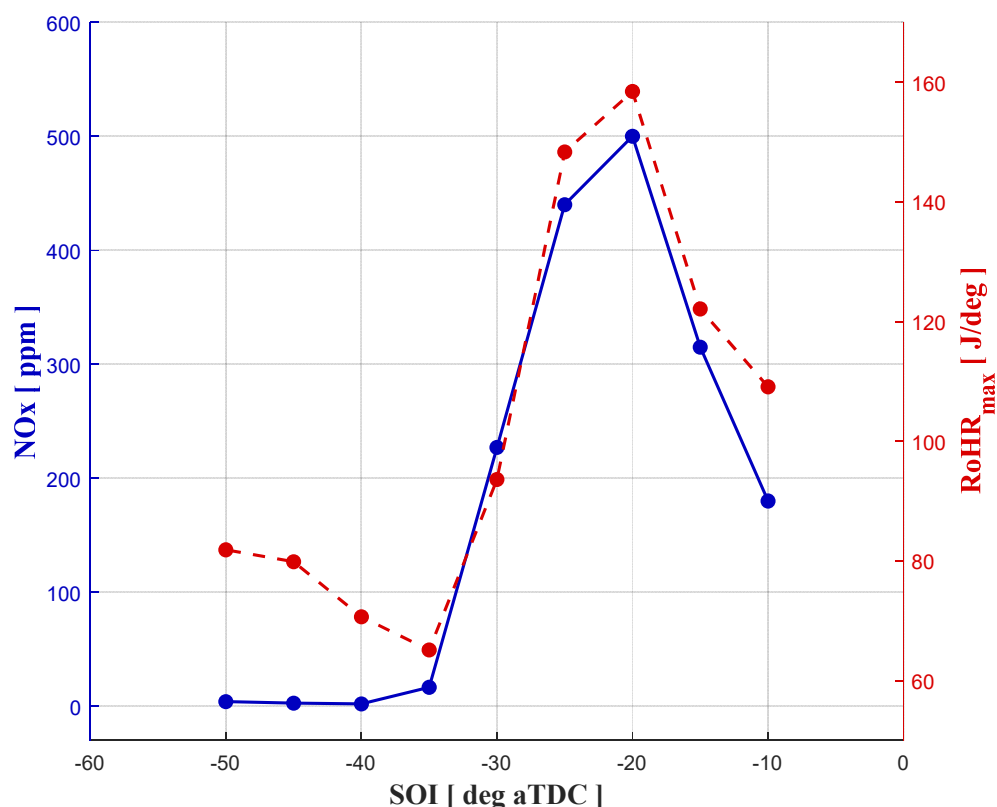


Figure 11. Average NOx-RoHR_{max} correlation obtained through slow speed pollutant measurement (Richmond measurement system) running a SOI sweep in dual-fuel mode at low-load.

Following the same approach described in the previous section for identifying the HC-IMEP correlation, the fast NO_x signal was acquired and synchronized with the EVO (after compensating for time-delay as discussed above). By phasing the instantaneous NO_x emissions with the exhaust stroke, it was possible to clearly identify the NO_x emissions associated with each engine cycle. Since the signal output characteristics of the CAMBUSTION CLD500 have the same features as the fast HC analyzer, the same signal processing (acquisition and filtering) was adopted. Figure 12 shows the CAMBUSTION CLD500 signal (red line) and in-cylinder pressure signal (blue line) of an engine cycle characterized by high NO_x emission (retarded SOI −20 deg aTDC).

Figure 12 clearly shows the peak of NO_x emissions placed at the end of expansion stroke (EVC −355 deg aTDC) which can be assumed as the cyclic NO_x production. Such behavior can be related to the delay of the Fast NO_x before starting to measure the exhaust gases of the actual cycle. As documented by Peckham et al. [37] and Schurov et al. [38], the evident instantaneous NO_x signal drop reported in Figure 12, around EVO, is related to the residence time of the exhaust gases behind the valve. The first portion of the gas sampled will be that which was released at the end of the previous exhaust stroke and then stayed in the port throughout the entire exhaust valve closed period resulting in a low NO_x concentration. Moreover, since fast NO_x and fast FID data have the same characteristics in term of signal output, the cycle resolved data have a crank angle resolution of 16 degrees that contributes retarding the rise of NO_x signal.

With the aim of confirming the NO_x-RoHR_{max} correlation identified through the analysis of the average data in Figure 11, the two stage RoHR combustion region (SOI from −10 to −30 deg aTDC) was considered. As clearly shown in Figure 13, where a cycle-to-cycle comparison (300 consecutive engine cycles) between the maximum value of the instantaneous NO_x and the calculated RoHR_{max} was performed, the same trend reported in Figure 11 can be noticed. As discussed before, by advancing the SOI, the magnitude of the first RoHR stage initially increases and subsequently decreases, with

obvious consequences in terms of NO_x production. A further advancement in SOI generates near-zero NO_x production because of the different combustion behavior (Gaussian RoHR shape), confirming the link between the combustion RoHR shape and NO_x production. This strong linear correlation ($R^2 = 0.82$) between NO_x emissions and the transformation of the RoHR shape in dual-fuel combustion has been previously observed by several researchers, most recently by Partridge et al. [32], who attributed the RoHR shape transformation to local air–fuel ratio stratification.

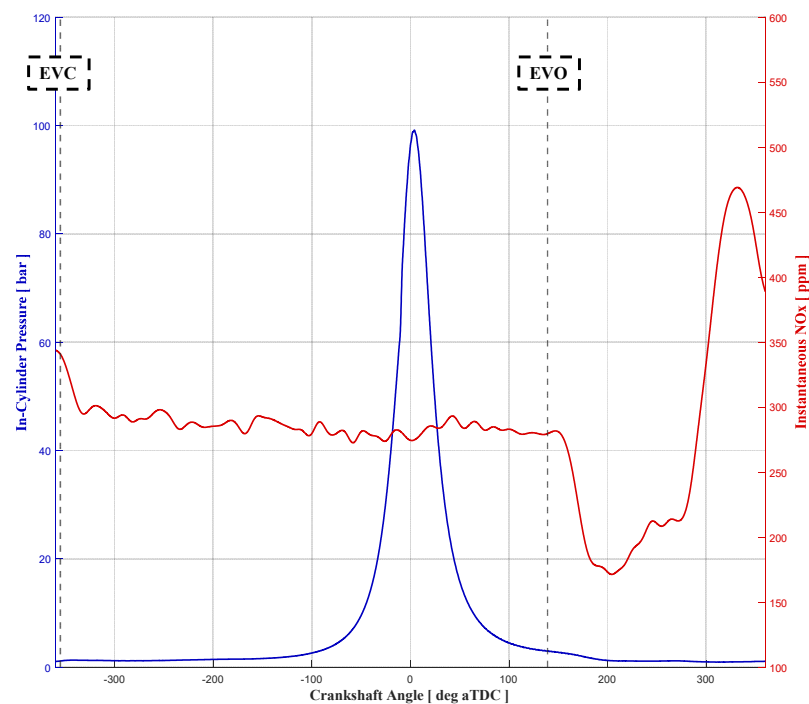


Figure 12. In-cylinder pressure signal and Instantaneous NO_x production for a dual-fuel engine operating condition at SOI -20 deg aTDC.

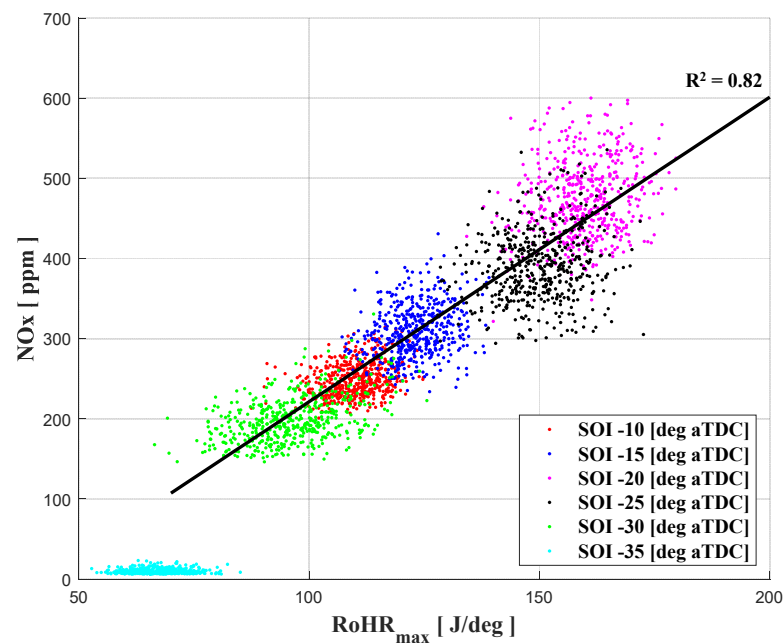


Figure 13. Cycle-to-cycle NO_x-RoHR_{max} correlation obtained through high-frequency pollutant measurement (CAMBUSTION measurement system) running a SOI sweep in dual-fuel mode at low load.

5. Conclusions

This work highlights the correlation between combustion characteristics and pollutants emissions, especially unburned hydrocarbons (HC) and oxides of nitrogen (NO_x) based on fast FID and fast NO_x measurements acquired cycle-by-cycle. The experimental investigation was performed on a Single-Cylinder Research engine run in dual-fuel diesel–natural gas mode at a fixed speed and a fixed low load of 5 bar IMEP gross and 1339 rpm, respectively. The natural gas PES was kept constant at 80% and the diesel was injected at an injection pressure of 500 bar, while the HRF SOI was varied from -10 to -60 deg aTDC.

The instantaneous pollutants emissions were acquired using CAMBUSTION HFR400 and CLD 500 with sampling frequency of 500 Hz able to obtain cycle-resolved data. To further validate the values coming from the CAMBUSTION instrumentations, a standard five-gas emission bench was used to compare the outputs in terms of average (steady-state) pollutants concentrations from different sources. Once compensated for the time-delay of the fast emission measurement systems with respect to the actual engine cycle (due to the distance between the exhaust valve and the sampling probe), the analysis of the acquired data allowed to define two correlations aimed at demonstrating the sources of each pollutants produced.

The correlation between cycle-to-cycle variability and the HC production were identified by comparing two different engine operating conditions of -10 deg aTDC and -60 deg aTDC, called “Retarded SOI” and “Advanced SOI”, respectively. Introducing the Net Cyclic Hydrocarbon (NCHC) emissions as representative of the net HC production (if positive), or net HC reduction (if negative), for the analyzed engine cycle compared to the previous one, the cyclic variability was defined through the calculation of the IMEP difference between of two consecutive engine cycles (Δ IMEP). Finally, a linear experimental correlation ($R^2 = 0.86$) between NCHC and Δ IMEP was obtained, providing a reasonable physical explanation for high HC emission running diesel–NG dual-fuel combustion at low load with advanced injection timing.

Following the same approach, a physical explanation for high NO_x emissions in diesel–NG dual-fuel combustion was proposed. Through the analysis of the ensemble-averaged RoHR data and slow-speed measurements, a potential link between the combustion shape (i.e., the existence of a distinct first stage of RoHR, summarized by the RoHRmax) and NO_x emissions was identified. The analysis of the cycle-to-cycle combustion data and crank-resolved NO_x measurements confirmed the existence of a clear trend through the identification of a linear correlation ($R^2 = 0.82$) between the maximum value of the instantaneous NO_x and the calculated RoHRmax. Since the analysis performed in this paper consider only few SOIs at a constant load (low load), further activities are currently being performed to verify the obtained correlation at different engine operating conditions of RPM, load, intake pressure, rail pressure and number of HRF injections.

Author Contributions: Conceptualization, G.S., K.K.S. and S.R.K.; methodology, G.S. and A.N. and F.P.; investigation, G.S., A.N., N.C. and S.R.K.; resources, G.S. and A.N.; data curation, G.S.; writing—original draft preparation, G.S. and V.R. writing—review and editing, K.K.S., S.R.K., F.P. and P.P.; visualization, G.S. and V.R.; supervision, F.P., S.R.K. and K.K.S.; project administration, V.R., F.P., S.R.K. and K.K.S. All authors have read and agreed to the published version of the manuscript.

Funding: This paper was developed based on partial funding from the Alliance for Sustainable Energy, LLC, Managing and Operating Contractor for the National Renewable Energy Laboratory for the U.S. Department of Energy (Prime Award #DE-AC36-08GO28308; Subaward #NHQ-9-82305-01). Additional financial support was provided by the Department of Mechanical Engineering of The University of Alabama, and the University of Bologna.

Data Availability Statement: The data presented in this paper will be provided by the authors on request.

Acknowledgments: The authors acknowledge funding from the Alliance for Sustainable Energy, LLC, Managing and Operating Contractor for the National Renewable Energy Laboratory for the U.S. Department of Energy as well as from the University of Bologna and The University of Alabama.

Conflicts of Interest: The authors declare no conflict of interest.

Abbreviations

Ac	Alternate current
aTDC	after Top Dead Center
bTDC	before Top Dead Center
CAD	Crank Angle Degree
CDC	Conventional Diesel Combustion
CO	Carbon Oxides
COV imep	Coefficient of Variation of IMEP
dV	Derivative Volume
dp	Derivative Pressure
EVC	Exhaust Valve Closing angle
EVO	Exhaust Valve Opening angle
FCE	Fuel Conversion Efficiencies
HCS	Unburned Hydrocarbons
HCCI	Homogeneous Charge Compression Ignition
HP	Horse Power
HRF	High-Reactivity Fuel
IMEP	Indicated Mean Effective Pressure
ISFC	Indicated Specific Fuel Consumption
IVC	Intake Valve Closing angle
IVO	Intake Valve Opening angle
LHV _{LRF}	Low Heating Value of Low Reactivity Fuel
LHV _{HRF}	Low Heating Value of High Reactivity Fuel
LRF	Low-Reactivity Fuel
LTC	Low-Temperature Combustion
LTHR	Low-Temperature Heat Release
MBT	Maximum Brake Torque
NCHC	Net Cyclic Hydrocarbons
NG	Natural Gas
NOx	Oxides of Nitrogen
P	Pressure
PES	Percentage Energy Substitution
PREMIER	Premixed Mixture Ignition in the End-gas Region
POMDME	Polyoxymethylene di-methyl ether
RCCI	Reactivity Controller Compression Ignition
RoHR	Rate of Heat Release
RoHRmax	Maximum Rate of Heat Release
SOI	Start of Injection angle
TDC	Top Dead Center
V	Volume
Δ IMEP	Cyclic IMEP variation
\dot{m}_{HRF}	High-Reactivity Fuel Flowrate
\dot{m}_{LRF}	Low-Reactivity Fuel Flowrate
γ	Adiabatic index

References

1. Thring, R. *Homogeneous-Charge Compression-Ignition (HCCI) Engines*; SAE Technical Paper 892068; SAE: Warrendale, PA, USA, 1989. [[CrossRef](#)]
2. Christensen, M.; Johansson, B. *Supercharged Homogeneous Charge Compression Ignition (HCCI) with Exhaust Gas Recirculation and Pilot Fuel*; SAE Technical Paper 2000-01-1835; SAE: Warrendale, PA, USA, 2000. [[CrossRef](#)]
3. Imamoto, T.; Kawahara, N.; Tomita, E. PREMIER combustion characteristics of a pilot fuel-ignited dual-fuel biogas engine with consideration of cycle-to-cycle variations. *Fuel* **2022**, *314*, 123049. [[CrossRef](#)]

4. Azimov, U.; Tomita, E.; Kawahara, N.; Harada, Y. Premixed mixture ignition in the end-gas region (PREMIER) combustion in a natural gas dual-fuel engine: Operating range and exhaust emissions. *Int. J. Engine Res.* **2011**, *12*, 484–497.
5. Shin, J.; Choi, J.; Seo, J.; Park, S. Pre-chamber combustion system for heavy-duty engines for operating dual fuel and diesel modes. *Energy Convers. Manag.* **2022**, *255*, 115365. [[CrossRef](#)]
6. Salahi, M.M.; Esfahanian, V.; Gharehghani, A.; Mirsalim, M. Investigating the reactivity controlled compression ignition (RCCI) combustion strategy in a natural gas/diesel fueled engine with a pre-chamber. *Energy Convers. Manag.* **2017**, *132*, 40–53. [[CrossRef](#)]
7. Kokjohn, S.; Hanson, R.; Splitter, D.; Kaddatz, J.; Reitz, R. Fuel Reactivity Controlled Compression Ignition (RCCI) Combustion in Light- and Heavy-Duty Engines. *SAE Int. J. Engines* **2011**, *4*, 360–374.
8. Hanson, R.; Kokjohn, S.; Splitter, D.; Reitz, R. Fuel Effects on Reactivity Controlled Compression Ignition (RCCI) Combustion at Low Load. *SAE Int. J. Engines* **2011**, *4*, 394–411.
9. Paykani, A.; Garcia, A.; Shahbakhti, M.; Rahnama, P.; Reitz, R.D. Reactivity controlled compression ignition engine: Pathways towards commercial viability. *Appl. Energy* **2021**, *282*, 116174.
10. Benajes, J.; García, A.; Monsalve-Serrano, J.; Villalta, D. Exploring the limits of the reactivity controlled compression ignition combustion concept in a light-duty diesel engine and the influence of the direct-injected fuel properties. *Energy Convers. Manag.* **2018**, *157*, 277–287.
11. Kakaee, A.; Rahnama, P.; Paykani, A. Numerical Study of Reactivity Controlled Compression Ignition (RCCI) Combustion in a Heavy-Duty Diesel Engine Using 3D-CFD Coupled with Chemical Kinetics. *Int. J. Automot. Eng.* **2014**, *4*, 792–804.
12. Reitz, R.D.; Duraisamy, G. Review of high efficiency and clean reactivity controlled compression ignition (RCCI) combustion in internal combustion engines. *Prog. Energy Combust. Sci.* **2015**, *46*, 12–71.
13. Krishnan, S.; Srinivasan, K.; Singh, S.; Bell, S.; Midkiff, K.; Gong, W.; Fiveland, S.; Willi, M. Strategies for Reduced NOx Emissions in Pilot-Ignited Natural Gas Engines. *ASME. J. Eng. Gas Turbines Power* **2004**, *126*, 665–671.
14. Raihan, M.; Guerry, E.; Dwivedi, U.; Srinivasan, K.; Krishnan, S. Experimental Analysis of Diesel-Ignited Methane Dual-Fuel Low-Temperature Combustion in a Single-Cylinder Diesel Engine. *J. Energy Eng.* **2014**, *141*, C4014007.
15. Krishnan, S.; Srinivasan, K.; Raihan, M. The effect of injection parameters and boost pressure on diesel-propane dual fuel low temperature combustion in a single-cylinder research engine. *Fuel* **2016**, *184*, 490–502.
16. Narayanan, A.; Hariharan, D.; Partridge, K.; Pearson, A.; Srinivasan, K.; Krishnan, S. Impact of Low Reactivity Fuel Type and Energy Substitution on Dual Fuel Combustion at Different Injection Timings. *Energies* **2023**, *16*, 1807. [[CrossRef](#)]
17. Hariharan, D.; Partridge, K.; Narayanan, A.; Srinivasan, K. Strategies for Reduced Engine-Out HC, CO, and NOx Emissions in Diesel-Natural Gas and POMDME-Natural Gas Dual-Fuel Engine. *SAE Int. J. Adv. Curr. Prac. Mobil.* **2022**, *4*, 1264–1278.
18. Selim, M.Y.E. Effect of engine parameters and gaseous fuel type on the cyclic variability of dual fuel engines. *Fuel* **2005**, *84*, 961–971.
19. Ozdor, N.; Dulger, M.; Sher, E. *Cyclic Variability in Spark Ignition Engines A Literature Survey*; SAE Technical Paper 940987; SAE: Warrendale, PA, USA, 1994.
20. Hamai, K.; Kawajiri, H.; Ishizuka, T.; Nakai, M. *21st Symposium (International) on Combustion*; Technical University of Munich West Germany: München, Germany, 1986.
21. Galloni, E. Analyses about parameters that affect cyclic variation in a spark ignition engine. *Appl. Therm. Eng.* **2008**, *29*, 1131–1137. [[CrossRef](#)]
22. Matekunas, F. *Modes and Measures of Cyclic Combustion Variability*; SAE Technical Paper 830337; SAE: Warrendale, PA, USA, 1983.
23. Srinivasan, K.K.; Agarwal, A.K.; Krishnan, S.R.; Mulone, V. *Natural Gas Engines—For Transportation and Power*; Springer: Berlin/Heidelberg, Germany, 2019.
24. Jha, P.R.; Krishnan, S.R.; Srinivasan, K.K. Impact of methane energy fraction on emissions, performance and cyclic variability in low-load dual fuel combustion at early injection timings. *Int. J. Engine Res.* **2021**, *22*, 1255–1272.
25. Cheng, Q.; Ahmad, Z.; Kaario, O.; Martti, L. Cycle-to-cycle variations of dual-fuel combustion in an optically accessible engine. *Appl. Energy* **2019**, *254*, 113611.
26. Ravaglioli, V.; Carra, F.; Moro, D.; De Cesare, M.; Stola, F. *Remote Sensing Methodology for the Closed-Loop Control of RCCI Dual Fuel Combustion*; SAE Technical Paper 2018-01-0253; SAE: Warrendale, PA, USA, 2018. [[CrossRef](#)]
27. Curran, S.; Hanson, R.; Wagner, R.; Reitz, R. *Efficiency and Emissions Mapping of RCCI in a Light-Duty Diesel Engine*; SAE Technical Paper 2013-01-0289; SAE: Warrendale, PA, USA, 2013. [[CrossRef](#)]
28. Matsuura, K.; Iida, N. *Effect of Temperature-Pressure Time History on Auto-Ignition Delay of Air-Fuel Mixture*; SAE Technical Paper 2018-01-1799; SAE International: Warrendale, PA, USA, 2018. [[CrossRef](#)]
29. Silvagni, G.; Ravaglioli, V.; Falfari, S.; Ponti, F.; Mariani, V. Development of a Control-Oriented Ignition Delay Model for GCI Combustion. *Energies* **2022**, *15*, 6470. [[CrossRef](#)]
30. Ravaglioli, V.; Ponti, F.; Silvagni, G.; De Cesare, M. Development of a Methodology for the Investigation of Residual Gases Effects on Gasoline Compression Ignition. In Proceedings of the ASME 2020 Internal Combustion Engine Division Fall Technical Conference, Virtual, Online, 4–6 November 2020. [[CrossRef](#)]
31. Heywood, J. *Internal Combustion Engine Fundamentals*; McGraw-Hill Education: New York, NY, USA, 1988.
32. Partridge, K.; Jha, P.; Srinivasan, K.; Krishnan, S. An experimental and computational analysis of combustion heat release transformation in dual fuel combustion. *Fuel* **2023**, *341*, 127561. [[CrossRef](#)]

33. Shibata, G.; Oyama, K.; Urushihara, T.; Nakano, T. *Correlation of Low Temperature Heat Release with Fuel Composition and HCCI Engine Combustion*; SAE Technical Paper 2005-01-0138; SAE: Warrendale, PA, USA, 2005. [[CrossRef](#)]
34. Novella, R.; Pla, B.; Bares, P.; Jiménez, I. Acoustic characterization of combustion chambers in reciprocating engines: An application for low knocking cycles recognition. *Int. J. Engine Res.* **2022**, *23*, 120–131. [[CrossRef](#)]
35. Ravaglioli, V.; Ponti, F.; Carra, F.; Corti, E.; De Cesare, M.; Stola, F. Combustion Indexes for Innovative Combustion Control. *SAE Int. J. Engines* **2017**, *10*, 2371–2381. [[CrossRef](#)]
36. Del Vescovo, D.; Kokjohn, S.; Reitz, R. The Effects of Charge Preparation, Fuel Stratification, and Premixed Fuel Chemistry on Reactivity Controlled Compression Ignition (RCCI) Combustion. *SAE Int. J. Engines* **2017**, *10*, 1491–1505. [[CrossRef](#)]
37. Peckham, M.; Hands, T.; Burrell, J.; Collings, N.; Schurov, S. *Real Time In-Cylinder and Exhaust NO Measurements in a Production SI Engine*; SAE Technical Paper 980400; SAE: Warrendale, PA, USA, 1998. [[CrossRef](#)]
38. Schurov, S.; Collings, N.; Hands, T.; Peckham, M.; Burrell, J. *Fast Response NO/HC Measurements in the Cylinder and Exhaust Port of a DI Diesel Engine*; SAE Technical Paper 980788; SAE: Warrendale, PA, USA, 1998. [[CrossRef](#)]

Disclaimer/Publisher’s Note: The statements, opinions and data contained in all publications are solely those of the individual author(s) and contributor(s) and not of MDPI and/or the editor(s). MDPI and/or the editor(s) disclaim responsibility for any injury to people or property resulting from any ideas, methods, instructions or products referred to in the content.